Collective excitations and shape changes in ^{80}Y

R. A. Kaye,[1,2] O. Grubor-Urosevic,[1] S. L. Tabor,[2] J. Döring,[3] Y. Sun,[4,5] R. Palit,[3] J. A. Sheikh,[6] T. Baldwin,[2,*] D. B. Campbell,[2] C. Chandler,[2,†] M. W. Cooper,[2,‡] S. M. Gerbick,[1] C. R. Hoffman,[2] J. Pavan,[2] L. A. Riley,[7,§] and M. Wiedeking[2]

[1]*Department of Chemistry and Physics, Purdue University Calumet, Hammond, Indiana 46323, USA*

[2]*Department of Physics, Florida State University, Tallahassee, Florida 32306, USA*

[3]*Gesellschaft für Schwerionenforschung (GSI), Planckstr. 1, D-64291 Darmstadt, Germany*

[4]*Department of Physics and Joint Institute of Nuclear Astrophysics, University of Notre Dame, Notre Dame, Indiana 46556, USA*

[5]*Department of Physics, Xuzhou Normal University, Xuzhou, Jiangsu 221009, People's Republic of China*

[6]*Department of Physics, University of Kashmir, Hazrathbal, Srinagar, Kashmir 190 006, India*

[7]*Department of Physics and Astronomy, Earlham College, Richmond, Indiana 47374, USA*

(Received 24 January 2004; published 14 June 2004)

Lifetimes of 30 high-spin levels in ^{80}Y were measured using the Doppler-shift attenuation method. The high-spin states were populated using the ^{54}Fe(^{28}Si, *pn*) reaction at 90 MeV, with a thick 14 mg/cm^2 ^{54}Fe target used to stop all recoils. Prompt $\gamma-\gamma$ coincidences were detected using a Compton-suppressed Ge array consisting of three Clover detectors and seven single-crystal detectors. Lifetimes were determined from experimental line shapes measured at both 35° and 145° whenever possible. Transition quadrupole moments Q_t inferred from the lifetimes in the lowest positive- and negative-parity bands are large (>3 *e*b) at low spin, but show a rather abrupt decrease at high spin. Results of calculations using the projected shell and cranked Woods-Saxon models in conjunction with the cranked-shell model suggest that these drops in Q_t are due to quasiparticle alignment, which introduce shape changes in each band from nearly prolate below the alignment to triaxial above. Magnetic dipole transition strengths $B(M1)$ in the yrast positive-parity band show a strong alternating pattern with spin, similar to that observed in other neighboring odd-odd nuclei.

DOI: 10.1103/PhysRevC.69.064314 PACS number(s): 21.10.Tg, 21.10.Re, 23.20.Lv, 27.50.+e

I. INTRODUCTION

Odd-odd nuclei in the $f-p-g$ shell have demonstrated a systematic richness of structure that appears to be consistent across the entire shell [1]. Their yrast positive-parity bands are understood to be based on the $\pi g_{9/2} \otimes \nu g_{9/2}$ two-quasiparticle (2-qp) configuration, leading to very similar observed behaviors such as moments of inertia converging toward the rigid rotor value at high spin [2], asymmetric energy splitting between the odd and even spin states (signature splitting), alternating $B(M1)$ strengths with spin, and a reversal in the phase of the normalized energy differences between adjacent states. For the most part, many of these behaviors can be explained from a theoretical standpoint (see Refs. [3–5]). For example, the 2-qp plus rotor model [6] has demonstrated good qualitative agreement with the observed alternations in the normalized energy differences (signature splitting pattern) and the $B(M1)$ strengths with spin in ^{82}Y [4] and ^{78}Rb [7]. Recently, a systematic study of the yrast positive-parity bands in several odd-odd nuclei near the $N=Z$ line was performed [8] using the projected shell-model approach [9]. Like the 2-qp plus rotor model, there was good qualitative agreement between the calculated alternations and the measured ones. In both models, however, good quantitative agreement was difficult to achieve across the entire spin range in which experimental data were available. In particular, the observed systematic attenuation of the $B(M1)$ strengths with decreasing spin and the reversal in the phase of the signature splitting pattern were in general not well reproduced by the calculations, although comparisons were hindered by the relatively small number of lifetime measurements performed for $N \approx Z$ odd-odd nuclei [4,7,10–14]. More experimental lifetime information in the yrast positive-parity bands of other odd-odd nuclei in this region would provide additional tests of the available models and could help expand the understanding of their behavior with the evolution of spin.

The picture is less clear in the negative-parity bands, mostly because of strong Coriolis mixing among the *fp* orbitals which tends to cloud theoretical interpretations. Most of the same systematic behaviors observed for the yrast positive-parity bands are typically not seen in the yrast negative-parity bands. As an example, only modest alternations (if any) have been observed in both the signature splitting and $B(M1)$ strength patterns where data are available. However, changes in the signature splitting pattern appear to be consistent indicators of structure changes in these bands. In the yrast negative-parity band of ^{80}Y, the amount of signature splitting increases noticeably above spin 16, in harmony with a suggested $g_{9/2}$ neutron alignment [15], while in

*Present address: Department of Physics, University of Surrey, Guildford, Surrey, GU2 7XH, UK.

†Present address: School of Chemistry and Physics, Keele University, Keele, Staffordshire, ST5 5BG, UK.

‡Present address: National Superconducting Cyclotron Laboratory, Michigan State University, East Lansing, MI 48824.

§Present address: Department of Physics and Astronomy, Ursinus College, Collegeville, PA 19426.

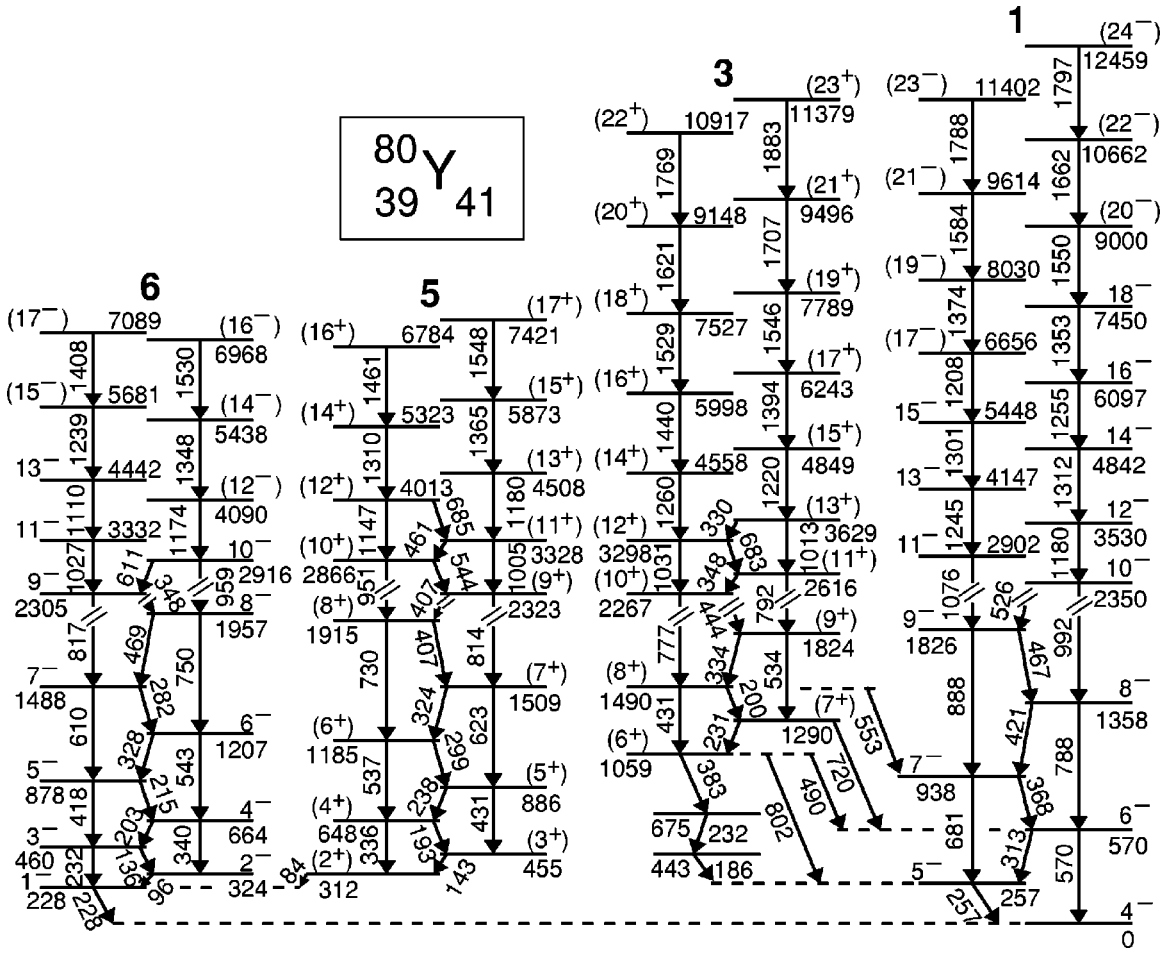

FIG. 1. Partial level scheme of ^{80}Y [15] showing the bands in which lifetimes were measured in the present work. The vertical energy scale is compressed by a factor of three above an excitation energy of 2000 keV. The numbers above the decay sequences are intended only to facilitate the discussion and follow the same convention as in Ref. [15].

a similar band in ^{72}Br, an inversion in the pattern occurs near the same spin, attributed [16] to a triaxial shape evolution and an unpaired band crossing. Detecting possible changes in collectivity in the same spin range could further illuminate the mechanisms associated with changes in the signature splitting pattern.

The goal of the present work was to measure as many mean lifetimes of excited states in ^{80}Y ($N=Z+2$) as possible in order to map the evolution of collectivity with spin for an odd-odd $N\approx Z$ nucleus, and to use this information to address the issues mentioned above. Until now, lifetime measurements had not been performed for any nonisomeric excited state in ^{80}Y, but the decay scheme has been well studied, formed by many complementary investigations. The initial identification of ^{80}Y [17] was determined by its β decay to states in ^{80}Sr. The existence of excited states had been mentioned [18] but not illustrated in a decay scheme until the emergence of a preliminary study which was never published [19]. A rich structure consisting of eight rotational bands was first revealed using the ^{24}Mg(^{58}Ni, pn) reaction [20] and later modified [21] by other experiments. During this time, the work of several independent studies [22–26] led to a more complete understanding of the low-lying portion of the level scheme, including the observation and half-life measurements of 1^- and (2^+) isomeric states at 228 and 312 keV, respectively, and a description of how these levels link some of the excited states to the ground state. The most recent investigation [15] extended the level scheme to spins as high as (24^-), and incorporated the clarifications at low spin provided by the previous complementary studies. A portion of the level scheme given in Ref. [15], relevant to the present work, is shown in Fig. 1.

Despite a relatively low maximum production cross section of about 20 mb (based on a theoretical PACE2 (projected angular-momentum coupled evaporation) calculation [27]), the use of a modern γ-detector array allowed for the measurement of several lifetimes in ^{80}Y using the Doppler-shift attenuation method (DSAM). As a result of this measurement, the degree of collectivity (or deformation) as a function of spin was mapped over several states in two rotational bands, and at least characterized for two other bands. It provided an additional case study for the emerging systematic trends of transition strength behavior for an odd-odd $N\approx Z$ nucleus in the proton-rich sector of the $f-p-g$ shell, and another test of the theories which predict this behavior. It also provided additional structure data for the daughter product following the β^+ decay of $N=Z$ ^{80}Zr, a waiting-point

nuclide in the rapid-proton capture (rp) process of nucleosynthesis [28,29].

II. EXPERIMENTAL TECHNIQUE

High-spin states in ^{80}Y were produced following the ^{54}Fe(^{28}Si, pn) fusion-evaporation reaction at 90 MeV using the Tandem-Superconducting LINAC accelerator at Florida State University (FSU). (The beam energy was chosen to optimize the production cross section of ^{80}Y according to PACE2 calculations and a measurement of the relative excitation function.) In order to optimize the experiment for the detection of Doppler-shifted γ-ray line shapes and hence the measurement of lifetimes using the DSAM, a thick 14 mg/cm^2 ^{54}Fe target was used to stop completely all recoiling nuclei. The average initial recoil velocity of ^{80}Y nuclei was 0.028c. Prompt γ-ray coincidences were detected using the FSU array of Compton-suppressed Ge detectors, consisting of three 4-crystal Clover detectors placed at 90° relative to the beam direction, and single-crystal detectors placed at 35° (two detectors), 90° (1), and 145° (4).

The collected data were sorted into 3000×3000 channel square $\gamma-\gamma$ coincidence matrices with a dispersion of 0.9 keV/channel. Line shapes measured at 35° (145°) were obtained from background-subtracted spectra projected from matrices consisting of coincidence events between 35° (145°) detectors and all other detectors. About 7.4×10^7 (1.8×10^8) coincidence pairs were collected in the 35° (145°) versus all detectors matrix. The distribution of counts/channel and the appropriate background level for each line shape were obtained from program GNUSCOPE, a Linux-based, menu-driven γ-analysis software package developed at FSU [30].

III. ANALYSIS METHOD

Mean lifetimes of excited states in the bands shown in Fig. 1 were measured by applying the DSAM to the experimental line shapes of coincident γ rays detected at 35° and 145°. The DSAM applied to this experiment involved a comparison of the decay time of the recoiling nuclei with their slowing-down time in a thick target. This comparison was carried out using the simulation code FITS [31] which integrates over the thickness of the target and determines a Gaussian distribution of recoil velocities (with a width that is 10% of the kinematic mean) at the time of decay, thus accounting for the evaporation of charged particles in the reaction. It corrects for direct feeding from up to four known higher-lying states and side feeding from one unknown state, as well as for finite detector solid angle and resolution, and the energy dependence of the reaction cross sections as the beam slows through the target. The nuclear and electronic stopping powers were obtained from program SRIM2000 [32,33].

By varying the lifetime of the parent state of interest, a set of theoretical line shapes was produced and compared with the measured Doppler-shifted spectrum at 35° and 145° to find the best fit. The lifetime which generated a curve that had the lowest reduced χ^2 when compared to the experimental spectrum was taken as the lifetime of that state. The uncertainty in the individual lifetimes measured at both angles was determined by finding the lifetime value above and below the best-fit value which increased the minimum reduced χ^2 value by one unit. The accepted lifetime values were determined from a weighted average (based on the number of detectors) of the individual lifetimes measured at both angles (see Table I). The uncertainties in the accepted lifetimes were deduced from either the standard deviation of the set of two individual lifetimes or the uncertainties in the individual lifetime fits, whichever was larger.

All line shapes were obtained from coincidence spectra of transitions gated from below (GFB) the transition of interest. It was not possible to obtain reliable line shapes from spectra gated from above the transitions of interest due to either limited statistics or interference from much stronger reaction products. Effective lifetimes, which do not include feeding corrections, were first determined for each line shape with adequate statistics. All line shapes were then refit with feeding corrections, with the exception of those from the highest fitted transition in each band, where only an upper-limit effective lifetime could be obtained. A comparison of fits to the 888 keV (band 1 transition) line shape with (mean lifetime) and without (effective lifetime) feeding corrections is shown in Fig. 2 for spectra measured at both 35° and 145°.

The feeding corrections used the effective lifetime of the state (or possibly multiple states) immediately above and one side-feeding state to feed the state of interest. Side-feeding times were determined from a procedure adopted for ^{81}Sr [31] where the highest measurable state for which a mean lifetime can be determined is given a short side-feeding time, with an increase of about 0.04 ps per MeV of deexcitation thereafter. This assumption has been applied to an isotope (^{82}Y [4]) as well as an isotone (^{78}Rb [13]) of ^{80}Y. The present study incorporated a side-feeding time of 0.01 ps for the 7450 keV 18^- state in band 1, with all other side-feeding times based on this value. This choice resulted in side-feeding times that were most consistent with those used in the same spin range in ^{78}Rb and ^{82}Y. In many cases, however, the resulting mean lifetimes were rather insensitive to the side-feeding time as long as the side-feeding intensity was small. The amount of direct and side feeding was determined from the γ-ray intensities given in Ref. [15], since the compound nucleus produced from the reaction used in that work (^{82}Zr) is the same as that produced from the reaction used in the present study, with a difference in excitation energy of only 1.2 MeV. Branching ratios, needed for the determination of transition strengths and quadrupole moments, were also deduced from these intensities.

The line-shape analysis was complicated by the fact that ^{80}Y has several closely spaced doublets in the decay scheme, some of which are in coincidence with each other (see Fig. 1). In some cases, it was possible to fit each transition without interference from other peaks by using a selective choice of gates. When it was not possible to resolve individual line shapes, a modified version of FITS was used to fit two overlapping line shapes simultaneously with theoretical line shapes properly scaled by the intensity of each γ ray. This procedure was shown to be effective under similar circumstances in ^{86}Nb [34], ^{81}Y [35], and ^{86}Zr [36]. Figure 3 shows

TABLE I. Effective and mean lifetimes measured for ^{80}Y. The effective lifetimes ($\tau_{\rm eff}$) and accepted mean lifetimes ($\tau_{\rm acc}$) represent the weighted average (based on the number of detectors) of the results measured at 35° and 145°. Excitation energies (E_x), γ-ray energies (E_γ), and spins were taken from Ref. [15].

E_x (keV)	I_i^π ($\hbar$)	I_f^π ($\hbar$)	E_γ (keV)	$\tau_{\rm eff}$ (ps)	$\tau_{35°}$ (ps)	$\tau_{145°}$ (ps)	$\tau_{\rm acc}$ (ps)
				Band 1			
9000	(20^-)	18^-	1550	0.12^{+29}_{-9}			<0.12[a]
7450	18^-	16^-	1353	0.33^{+16}_{-15}	0.26^{+18}_{-13}	0.25^{+18}_{-18}	0.25^{+18}_{-13}
6656	(17^-)	15^-	1208	0.36^{+31}_{-17}			<0.36[a]
6097	16^-	14^-	1255	0.37^{+27}_{-27}	0.30^{+46}_{-23}	0.10^{+5}_{-4}	0.17^{+12}_{-12}
5448	15^-	13^-	1301	0.38^{+10}_{-10}	0.25^{+21}_{-15}	0.123^{+5}_{-4}	0.16^{+8}_{-8}
4842	14^-	12^-	1312	0.44^{+14}_{-11}	0.12^{+10}_{-7}	0.19^{+30}_{-15}	0.17^{+14}_{-10}
4147	13^-	11^-	1245	0.48^{+13}_{-11}	0.32^{+49}_{-25}	0.17^{+8}_{-6}	0.22^{+10}_{-9}
3530	12^-	10^-	1180	0.47^{+15}_{-13}	0.21^{+36}_{-13}	0.13^{+9}_{-6}	0.16^{+11}_{-7}
2902	11^-	9^-	1076	0.49^{+10}_{-10}	0.18^{+10}_{-7}		0.18^{+10}_{-7}
2350	10^-	8^-	992	0.60^{+10}_{-8}	0.30^{+19}_{-13}	0.21^{+7}_{-6}	0.24^{+8}_{-7}
1826	9^-	7^-	888	1.08^{+15}_{-11}	0.50^{+20}_{-13}	0.52^{+9}_{-7}	0.51^{+9}_{-7}
1358	8^-	6^-	788	2.45^{+133}_{-62}	1.06^{+430}_{-49}	1.18^{+63}_{-32}	1.14^{+61}_{-31}
				Band 3			
7789	(19^+)	(17^+)	1546	0.20^{+20}_{-11}			<0.20[a]
7527	(18^+)	(16^+)	1529	0.20^{+9}_{-8}			<0.20[a]
6243	(17^+)	(15^+)	1394	0.14^{+4}_{-4}	0.11^{+25}_{-9}		0.11^{+25}_{-9}
5998	(16^+)	(14^+)	1440	0.27^{+28}_{-17}	0.08^{+32}_{-7}	0.10^{+32}_{-6}	0.09^{+29}_{-5}
4849	(15^+)	(13^+)	1220	0.35^{+13}_{-10}	0.23^{+22}_{-17}	0.15^{+11}_{-7}	0.18^{+13}_{-8}
4558	(14^+)	(12^+)	1260	0.36^{+15}_{-12}	0.14^{+19}_{-12}	0.18^{+17}_{-17}	0.17^{+16}_{-15}
3629	(13^+)	(11^+)	1013	0.48^{+8}_{-7}	0.30^{+26}_{-20}	0.25^{+6}_{-5}	0.27^{+6}_{-5}
3298	(12^+)	(10^+)	1031	0.45^{+8}_{-8}	0.42^{+36}_{-28}	0.16^{+4}_{-4}	0.25^{+15}_{-15}
2616	(11^+)	(9^+)	792	1.29^{+97}_{-38}	0.96^{+120}_{-38}	0.95^{+77}_{-32}	0.95^{+77}_{-32}
				Band 5			
4508	(13^+)	(11^+)	1180	0.28^{+13}_{-12}			<0.28[a]
4013	(12^+)	(10^+)	1147	0.37^{+9}_{-9}			<0.37[a]
3328	(11^+)	(9^+)	1005	0.33^{+6}_{-6}			<0.33[a]
2866	(10^+)	(8^+)	951	0.72^{+24}_{-24}		0.44^{+17}_{-12}	0.44^{+17}_{-12}
2323	(9^+)	(7^+)	814	1.57^{+47}_{-24}	1.30^{+900}_{-70}	0.92^{+44}_{-24}	1.05^{+50}_{-27}
				Band 6			
4442	13^-	11^-	1110	0.32^{+16}_{-13}			<0.32[a]
3332	11^-	9^-	1027	0.70^{+33}_{-19}	0.44^{+26}_{-16}		0.44^{+26}_{-16}
2916	10^-	8^-	959	0.59^{+18}_{-18}			<0.59[a]
2305	9^-	7^-	817	1.89^{+530}_{-78}		1.19^{+380}_{-55}	1.19^{+380}_{-55}

[a]Effective lifetime.

the result of a simultaneous fit to the 1013 and 1031 keV transitions in band 3.

IV. RESULTS

Lifetimes of 30 excited states were measured using the DSAM and are given in Table I. The effective lifetimes represent the weighted average (based on the number of detectors) of the results obtained from each of the two detector angles for which they could be measured. Mean lifetimes, which include feeding corrections, are given for each detector angle along with the accepted lifetime which also represents the weighted average of the results at each angle. If a reliable line shape could not be obtained at one angle, a lifetime result is not included in the table. In some cases, the selective gating used to eliminate contaminating peaks in the line shape spectra reduced the statistics enough to introduce rather large statistical uncertainties in the lifetime results given in Table I. However, despite these uncertainties, the results were obtained from mostly clean line shapes and are

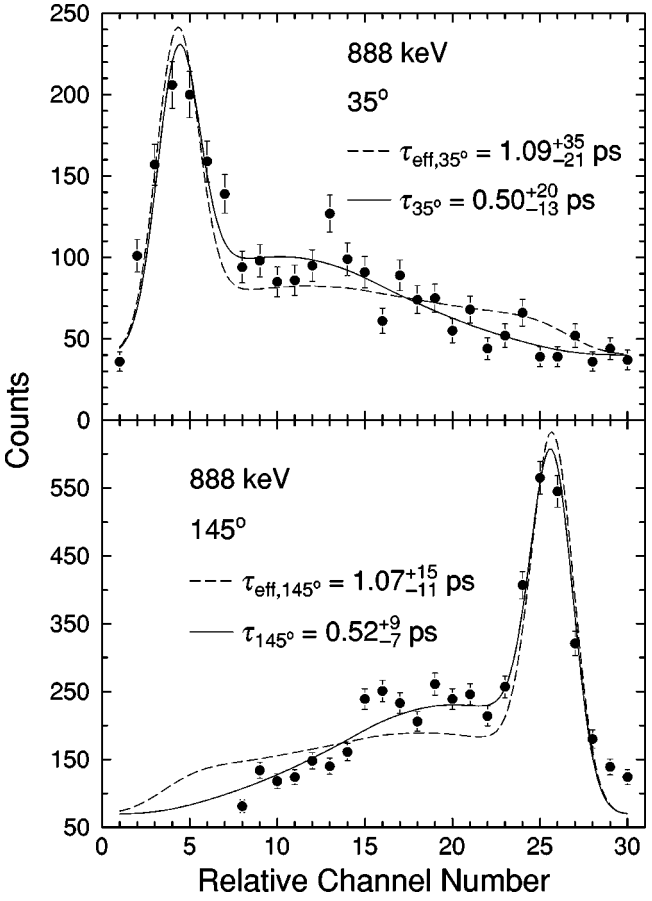

FIG. 2. Fits to the 35° and 145° line shapes of the 888 keV transition in band 1 with (solid line) and without (dashed line) feeding corrections. Each spectrum was obtained from a sum of gates on the 257 and 570 keV transitions in band 1.

therefore considered reliable. Figure 4 shows a sample of the lifetimes measured in band 1 of ^{80}Y.

A. Positive-parity states

Lifetimes were measured in the yrast positive-parity band (band 3 in Fig. 1) up to the (19^+) and (18^+) states in each signature by summing as many clean spectra GFB as possible. Line shapes could not be extracted above these levels, so only effective lifetimes are quoted for these states. Below these states, it was possible to fit line shapes and obtain mean lifetimes to as low as the (11^+) state. A simultaneous fit was performed to the 1013 and 1031 keV lines in order to decompose their line shapes and extract lifetimes individually for the (13^+) and (12^+) states, respectively (see Fig. 3). A line shape showing a small but detectable Doppler-shifted component was obtained for the 777 keV transition, but during the fitting process the corrected lifetime did not converge below 1.5 ps. Since the DSAM technique tends not to be as reliable above this value, a mean lifetime is not included for the (10^+) state. All γ rays emitted from the (9^+) and lower states showed no distinguishable Doppler shifting, and hence lifetimes could not be extracted from these transitions using the DSAM.

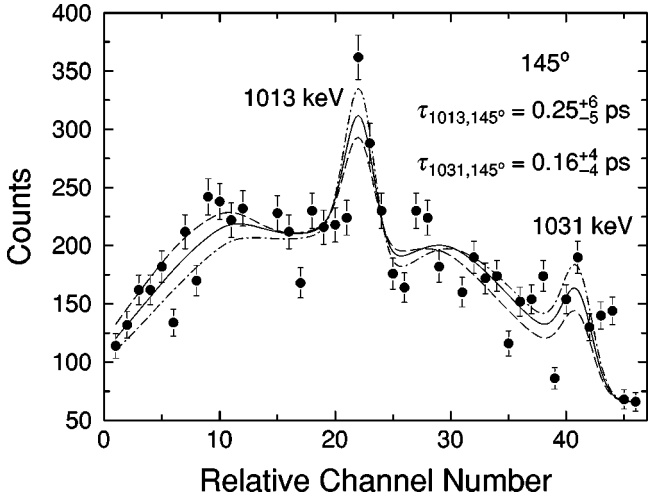

FIG. 3. Simultaneous fit to the line shapes of the 1013 and 1031 keV transitions in band 3 measured at 145°. The uncertainty limits of the overall best fit (solid curve) are indicated by the broken curves. The spectra were obtained from a sum of gates on the 257 and 802 keV transitions.

Three effective lifetimes and two mean lifetimes were also measured in a band based on the 312 keV (2^+) state (band 5 in Fig. 1). Despite summing several gates in this

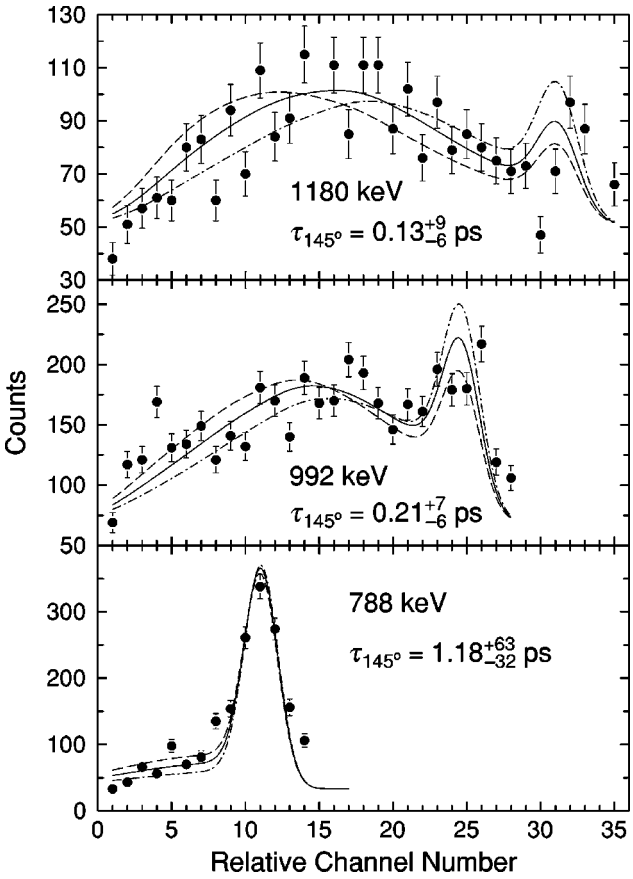

FIG. 4. Fits to the 145° line shapes of the 788, 992, and 1180 keV transitions in band 1. The uncertainty limits of the best fit (solid curve) are indicated by the broken curves.

band, reliable line shapes could not be extracted above the (13^+) and (12^+) states, and hence only effective lifetimes could be quoted for these levels. The shifted component of the 1005 keV transition appeared to consist of a multiplet of lines at both angles and with a variety of gate combinations, although a stopped component remained visible. Due to this uncertainty, feeding corrections were not invoked in this case and only an effective lifetime is given for the (11^+) state in this band.

B. Negative-parity states

Lifetimes were measured in the yrast negative-parity band (band 1 in Fig. 1) up to the (20^-) state, where an effective lifetime is given. The gates used to obtain the line shapes all showed coincidences with the 1245, 1255, 1301, and 1312 keV transitions. Thus, a simultaneous fit was performed to the line shapes of the 1245 and 1255 keV lines, as well as to the 1301 and 1312 keV lines, in order to resolve their individual line shape components. A slight Doppler-shifted component was observed for the 681 keV decay of the 7^- state, but a lifetime fit to this line shape did not converge below 2 ps, so evidently this lifetime cannot be measured by the DSAM. Below the 7^- state, there was no evidence of Doppler shifting.

The lifetimes of four states in a band based on the 228 keV 1^- state (band 6 in Fig. 1) were also measured. Three of these were measured in the $\alpha=1$ signature band, reflecting the fact that more reliable line shapes could be obtained from the more strongly populated odd-spin sequence.

C. Transition strengths

Reduced electric quadrupole transition strengths $B(E2)$ were determined from the accepted lifetimes given in Table I, and were used to calculate transition quadrupole moments $|Q_t|$ from the rotational model according to

$$Q_t^2 = \frac{16\pi}{5}\langle IK20|I-2K\rangle^{-2}B(E2, I\rightarrow I-2). \qquad (1)$$

Both the $B(E2)$ and Q_t values are given in Table II. The branching ratios and the values of the K spin projection quantum number used for each band [15] are also given in Table II.

Magnetic dipole transition strengths $B(M1)$ were calculated using a quadrupole-dipole mixing ratio of $\delta=0$ since $B(M1)$ values are rather insensitive to δ as long as it is small. Small values of δ have been observed systematically for $M1$ transitions in several neighboring odd-odd nuclei (^{78}Rb [13], for example), and are thus expected for similar $M1$ transitions in ^{80}Y. All deduced $B(M1)$ strengths are included in Table II.

V. DISCUSSION

The most recent high-spin study of ^{80}Y [15] demonstrated that this nucleus is similar in many ways to its odd-odd neighbors. The yrast band has positive parity based on the $\pi g_{9/2}\otimes\nu g_{9/2}$ intrinsic configuration, leading to several observed behaviors (based on the level energies and spins) that appear consistently in similar bands across this mass region (see Sec. I). Other similarities include a negative-parity yrare band and a rich band structure at high spin built upon several possible 2-qp intrinsic configurations.

However, there are also noticeable differences between the level scheme of ^{80}Y and those of its neighbors. Sequences of states appear more regular and form rotational bands at low spin more quickly than states of similar relative excitation energy in other odd-odd nuclei, such as the isotope ^{82}Y [4] and isotone ^{78}Rb [13]. There seems to be less mixing between states sharing the same parity, as indicated by a relatively small number of observed interband transitions. Moreover, the lowest negative-parity band (band 1 in Fig. 1) becomes increasingly closer to yrast with spin, particularly for the signature $\alpha=0$ sequence.

The lifetime measurements of this work provided another testing ground for possible similarities and a way to try to understand the differences between ^{80}Y and its neighboring odd-odd nuclei. These results also provided a direct comparison with the predictions from projected shell-model and cranked Woods-Saxon calculations. The results are discussed separately for the positive- and negative-parity bands below, following a brief overview of the models used to interpret the results.

A. Projected shell-model calculations

Calculations have been performed within the context of the projected shell model (PSM) [9] in order to investigate further the collective properties of the yrast positive-parity band in ^{80}Y. Previous calculations using the PSM [8] reproduced nicely the observed signature splitting between adjacent states in this band (see Fig. 2 in Ref. [8]), but could not describe the fine structure of signature inversion in the same band, as discussed in Ref. [8]. Only predictions of the $B(M1)/B(E2)$ ratios could be given at the time due to the lack of experimental lifetime measurements.

The PSM uses a rotational-invariant Hamiltonian including quadrupole-quadrupole, monopole-pairing, and quadrupole-pairing interaction terms. The strength of the quadrupole-quadrupole force was chosen so that the self-consistent relation with the input deformation parameter is kept. The monopole-pairing force strength took the form

$$G_M = \left[G_1 - G_2\frac{N-Z}{A}\right]A^{-1}, \qquad (2)$$

where $G_1=20.25$ for both neutrons and protons, and $G_2=16.20$ (0) for neutrons (protons). The quadrupole-pairing strength, assumed to be proportional to the monopole strength, was 16% of the monopole-pairing strength. These strengths are the same as those employed in the previous PSM calculations for this mass region [8].

In the calculations, the deformed qp basis is constructed from the Nilsson single-particle states followed by a BCS calculation. The single-particle space includes all nucleons in the $N=2,3,$ and 4 major shells. To build the shell-model basis for an odd-odd nucleus, the quasineutron and quasiproton

TABLE II. Energies, spins, γ-ray energies, branching ratios R_B, electric quadrupole transition strengths $B(E2)$, magnetic dipole transition strengths $B(M1)$, and transition quadrupole moments $|Q_t|$ in ^{80}Y. Energies and spins were taken from Ref. [15]. Values of the K spin projection quantum number used for each band are included.

E_x (keV)	I_i^π ($\hbar$)	E_γ (keV)	R_B (%)	$B(E2)$[a] (W.u.)	$B(M1)$ μ_N^2	$\lvert Q_t\rvert$ (eb)
Band 1			$K=4$			
9000	(20^-)	1550	100	>37[b]		>1.53[b]
7450	18^-	1353	100	35^{+38}_{-15}		1.15^{+67}_{-36}
6656	(17^-)	1208	100	>43[b]		>1.68[b]
6097	16^-	1255	100	75^{+181}_{-31}		2.25^{+190}_{-53}
5448	15^-	1301	100	67^{+67}_{-22}		2.15^{+89}_{-39}
4842	14^-	1312	100	60^{+86}_{-27}		2.07^{+116}_{-54}
4147	13^-	1245	100	61^{+42}_{-19}		2.12^{+64}_{-36}
3530	12^-	1180	100	109^{+85}_{-44}		2.91^{+97}_{-67}
2902	11^-	1076	100	154^{+98}_{-55}		3.56^{+100}_{-71}
2350	10^-	992	98	169^{+70}_{-42}		3.91^{+74}_{-52}
		526	2		0.03^{+1}_{-1}	
1826	9^-	888	94	133^{+21}_{-20}		3.69^{+28}_{-29}
		467	6		0.07^{+1}_{-1}	
1358	8^-	788	88	101^{+38}_{-35}		3.54^{+61}_{-68}
		421	12		0.08^{+3}_{-3}	
Band 3			$K=5$			
7789	(19^+)	1546	100	>22[b]		>1.23[b]
7527	(18^+)	1529	100	>24[b]		>1.28[b]
6243	(17^+)	1394	100	69^{+309}_{-48}		2.21^{+297}_{-99}
5998	(16^+)	1440	100	72^{+89}_{-54}		2.28^{+114}_{-117}
4849	(15^+)	1220	100	82^{+65}_{-34}		2.49^{+85}_{-59}
4558	(14^+)	1260	100	74^{+553}_{-36}		2.42^{+464}_{-68}
3629	(13^+)	1013	93	129^{+29}_{-23}		3.30^{+36}_{-31}
		330	7		0.41^{+9}_{-8}	
3298	(12^+)	1031	94	129^{+193}_{-48}		3.43^{+199}_{-72}
		683	6		0.04^{+6}_{-2}	
2616	(11^+)	792	76	103^{+52}_{-46}		3.23^{+74}_{-83}
		348	24		0.34^{+17}_{-15}	
Band 5			$K=2$			
4508	(13^+)	1180	100	>62[b]		>1.97[b]
4013	(12^+)	1147	83	>45[b]		>1.69[b]
		685	17		>0.08[b]	
3328	(11^+)	1005	81	>96[b]		>2.49[b]
		461	19		>0.34[b]	
2866	(10^+)	951	86	100^{+38}_{-28}		2.58^{+45}_{-39}
		544	14		0.11^{+4}_{-3}	
2323	(9^+)	814	72	77^{+26}_{-25}		2.30^{+37}_{-41}
		407	28		0.23^{+8}_{-7}	
Band 6			$K=1$			
4442	13^-	1110	100	>74[b]		>2.11[b]
3332	11^-	1027	100	79^{+45}_{-29}		2.20^{+56}_{-46}
2916	10^-	959	68	>57[b]		>1.88[b]

TABLE II. (*Continued.*)

E_x (keV)	I_i^π ($\hbar$)	E_γ (keV)	R_B (%)	$B(E2)$[a] (W.u.)	$B(M1)$ μ_N^2	$\lvert Q_t \rvert$ (eb)
		611	32		>0.14[b]	
2305	9^-	817	78	72^{+62}_{-55}		2.13^{+78}_{-109}
		348	22		0.25^{+21}_{-19}	

[a]W.u. = 20.5 e^2 fm^4.
[b]Based on an effective lifetime value.

creation operators are applied to the qp-vacuum state, and the resulting set of 2-qp states are projected onto good angular momentum states. The projected basis is used to diagonalize the shell-model Hamiltonian. The resulting eigenstates (wave functions) are used to determine transition strengths [37], and the $B(E2)$ strengths are used to calculate transition quadrupole moments according to Eq. (1). An effective charge of 1.8e (0.8e) was used for protons (neutrons). Calculations with smaller effective charges were performed, but these resulted in less qualitative agreement with the experimental results. More details about the PSM calculations can be found in Ref. [8]. Comparisons between the PSM predictions for ^{80}Y and the measured results are discussed in Sec. V C.

B. Cranked Woods-Saxon calculations

Cranked Woods-Saxon (CWS) calculations have been performed previously for ^{80}Y [23] in order to understand the microscopic characteristics of the ground state. The results indicated a strong prolate-deformed shape with an associated quadrupole deformation $\beta_2 \approx 0.38$, and provided further evidence for the 4^- ground state formed by the $\pi[422]5/2^+ \otimes \nu[301]3/2^-$ 2-qp configuration based on similar calculations and experimental evidence obtained for ^{79}Sr [38] and ^{81}Y [39,40].

In this work, the evolution of shape and deformation with rotational frequency has been calculated using the CWS approach for the lowest positive- and negative-parity bands, as well as for intrinsic configurations representing non-yrast states. The calculations generate a total Routhian surface (TRS) plot in the (β_2, γ) plane at discrete rotational frequencies, using a deformed Woods-Saxon potential and a short-range monopole pairing force [41]. At each grid point, the Routhian was minimized with respect to the hexadecapole deformation β_4.

Figure 5 shows six TRS plots at three different rotational frequencies (and their corresponding spin I) for intrinsic con-

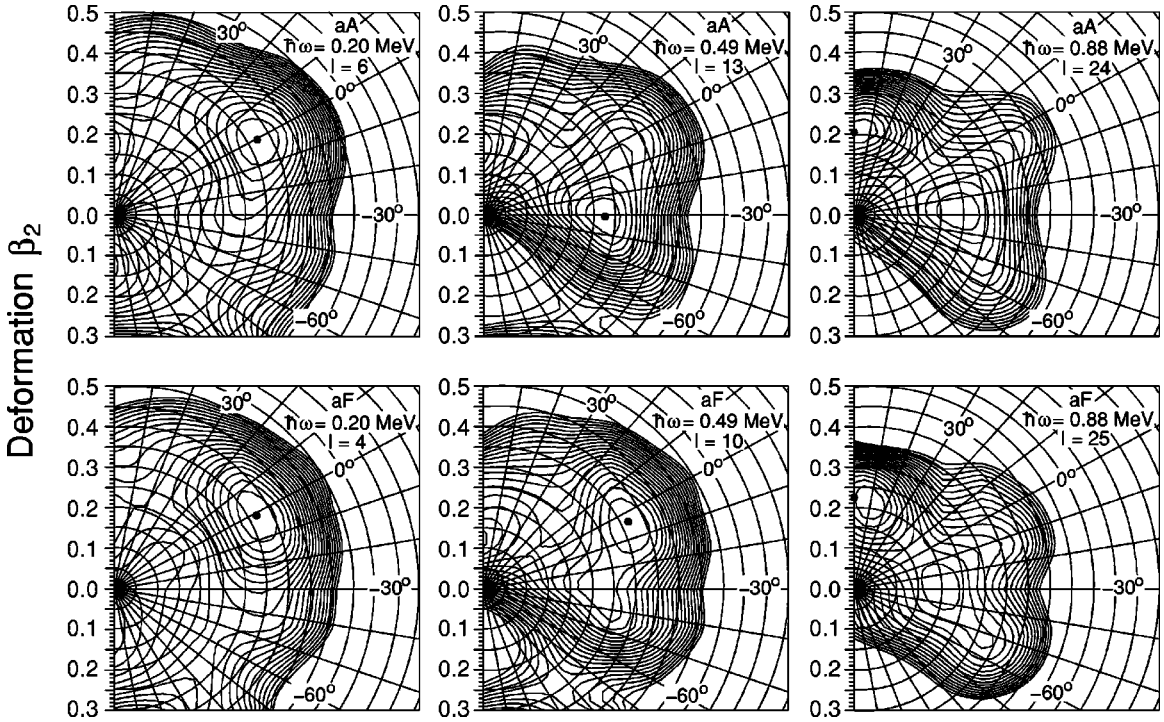

FIG. 5. Sample total Routhian surface plots for the lowest positive- and negative-parity configurations in ^{80}Y at three rotational frequencies (and their corresponding spin I) as indicated in each plot. The aA configuration corresponds to $(\pi, \alpha) = (+, 1)$ (odd spins in band 3), and the aF configuration corresponds to $(\pi, \alpha) = (-, 1)$ (odd spins in band 1). The spacing between contour lines is 200 keV.

figurations corresponding to the lowest positive- and negative-parity bands. The qp-labeling scheme of Ref. [42] was used, where lower (upper) case letters are used for the proton (neutron) configuration. Thus, the *aA* (*aF*) case stands for the lowest proton and neutron configuration yielding overall positive (negative) parity and signature $\alpha=1$.

At low spin, both configurations appear to have well deformed ($\beta_2\approx0.38$), nearly prolate ($\gamma\approx0°$) shapes. As the spin increases, the *aA* configuration shows a rather abrupt change in shape and deformation near spin 13, as shown in Fig. 5, evolving to a nearly triaxial shape ($\gamma\approx-30°$) with smaller deformation ($\beta_2\approx0.28$). In contrast, the *aF* configuration remains relatively unchanged near this spin, although the shape becomes noticeably more γ soft. When the spin is near the maximum observed experimentally ($I=24$), both configurations show a collective triaxial minimum with modest deformation. Comparisons between the deformations predicted from the CWS calculations and those inferred from the lifetimes are discussed in Secs. V C and V D.

The behavior of the TRS plots corresponding to non-yrast configurations having both positive and negative parity is qualitatively similar to those of their lower-energy counterparts. Large near-prolate deformation at low spin evolves to shapes with smaller deformation above $I\approx15$. Of the configurations tested, those having positive parity typically demonstrated somewhat larger deformation at low spin ($\beta_2\approx0.40$) than those having negative parity ($\beta_2\approx0.37$). The positive-parity configurations also seemed to favor triaxial shapes at high spin, while the negative-parity configurations showed coexisting triaxial and oblate shapes in the same spin range. However, the degree of γ softness was larger in all non-yrast configurations than those of their lower-energy counterparts shown in Fig. 5.

Theoretical Q_t values were calculated for each band in which lifetimes were measured by using the β_2 values obtained from the TRS plots. In order to make a proper comparison between experimental and theoretical values, the quadrupole deformation of the nuclear matter distribution derived from the TRS calculations was first related to the charge quadrupole deformation derived from the $B(E2)$ strengths [43,44]. In order to take triaxiality into account, the high-spin limit for the γ dependence of Q_t [45,46] was used to determine the accepted theoretical Q_t values from those calculated assuming axial symmetry [43].

C. Positive-parity bands

The transition quadrupole moments Q_t deduced from the measured lifetimes of yrast positive-parity states (band 3 in Fig. 1) are shown graphically in the bottom panel of Fig. 6. The results imply rather large collectivity below the (14^+) state, corresponding to an average quadrupole deformation $\beta_{2,\mathrm{ave}}=0.37$ in a rotational model picture, with a rather sudden reduction occurring at the (14^+) state. Above this state, the Q_t values remain relatively constant near an average value of 2.35 eb ($\beta_{2,\mathrm{ave}}=0.27$ assuming axial symmetry). The spin at which this reduction in collectivity takes place corresponds roughly to the crossing frequency at which a $g_{9/2}$ proton alignment occurs in each signature [15], as indicated

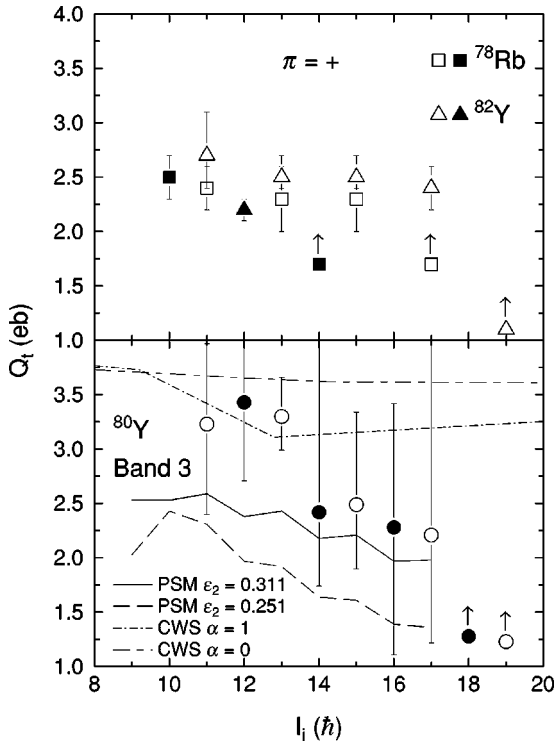

FIG. 6. Transition quadrupole moments Q_t as a function of the initial-state spin I_i for the yrast positive-parity bands of ^{78}Rb [13] and ^{82}Y [4] (top), and yrast positive-parity band 3 in ^{80}Y (bottom). Filled (open) symbols represent values obtained from signature $\alpha=0$ ($\alpha=1$) transitions. Symbols with arrows indicate lower limits established from effective lifetimes. The curves represent theoretical predictions from projected shell-model (PSM) and cranked Woods-Saxon (CWS) calculations, as indicated in the figure.

by an upbend in the kinematic moment of inertia $J^{(1)}$ near $\hbar\omega=0.7$ MeV (Fig. 10 in Ref. [15]), or about spin 17. Although the drop in Q_t begins at a spin smaller than the observed alignment, the two events are likely correlated considering that the changes in $J^{(1)}$ are rather broad (particularly in the $\alpha=1$ sequence) and probably represent a gradual qp alignment, since a "first-order" alignment is Pauli blocked for both unpaired nucleons.

The predicted Q_t values of the yrast positive-parity band according to the PSM calculations (see Sec. V A) are also shown in the bottom panel of Fig. 6. Two sets of calculations are given, corresponding to two different deformations where the model space is built. The absolute PSM values are clearly smaller than the observed ones. (Larger effective charges, if used in the calculations, can make a global enhancement in theoretical Q_t values. We do not prefer to do so as long as the qualitative behavior of the trend in Q_t can be understood.) The observed sudden drop in Q_t is not well reproduced by the calculations, however there is fair qualitative agreement between the experimental and predicted values. The largest collectivity is predicted at low spins and becomes reduced at higher spins, although the reduction in Q_t is much more gradual than the measured values. The Q_t values with the larger quadrupole deformation ϵ_2 can better reproduce the data, particularly for the higher spin states. This deformation ($\epsilon_2=0.311$) was used in Ref. [8] where the PSM calculations

for odd-odd nuclei in this mass region were first studied. The reason why we performed another calculation with a smaller deformation will be discussed later.

Band 3 has been suggested [15] to be based on the $\pi[422]5/2^+ \otimes \nu[422]5/2^+$ intrinsic configuration, with each qp occupying the first available orbital with positive parity above the deformed shell gap at nucleon number 38 near a prolate deformation of 0.38 [41]. The next lowest high-Ω single-particle orbital is the $[413]7/2^+$ one, which lies nearly 2 MeV above the $[422]5/2^+$ orbital at this deformation. The wave functions from the PSM calculations show strong mixing between the $\Omega=5/2$ and $\Omega=7/2$ prolate-deformed orbitals, especially as the spin increases. Considering that qp occupation of the $[413]7/2^+$ orbital tends to drive the nucleus toward smaller deformation, it is conceivable that the introduction of larger amplitudes of this high-Ω component to the wave function (manifested by a gradual $g_{9/2}$ proton alignment) is responsible for the observed reduction in the Q_t values.

The Q_t moments of band 3 as predicted by CWS calculations (see Sec. V B) are also superimposed with the experimental results in the bottom panel of Fig. 6. While there is good quantitative agreement between the predicted and experimental values below the (14^+) state, the observed drop in Q_t is not reproduced by the calculations. According to this model, a reduction in Q_t (or deformation) for both signatures is associated with a change in shape from predominantly prolate at lower spin to triaxial at higher spin (see Fig. 5). Considering the qualitative agreement between the variations in the $J^{(1)}$ and predicted Q_t values for each signature in this band, this shape change is likely a consequence of the gradual $g_{9/2}$ proton alignment.

The behavior of the Q_t moments above spin 9 for the yrast positive-parity bands in ^{78}Rb [7,13] and ^{82}Y [4,11,12] is displayed in the top panel of Fig. 6. In both cases, the Q_t moments show no sign of a drop above the 13^+ states (excluding the lower limits established from effective lifetimes), in contrast with those observed for band 3 in ^{80}Y (bottom panel of the same figure). However, neither ^{78}Rb nor ^{82}Y indicate evidence for qp alignment up to the highest observed transitions in their yrast bands based on the behavior of the $J^{(1)}$ values [4,13], and more Q_t moments were measured at higher spin in ^{80}Y than in ^{78}Rb and ^{82}Y. According to CWS calculations, the predicted shapes of ^{78}Rb and ^{82}Y associated with the yrast configuration also showed no evidence for a structure change, remaining consistently near-prolate (^{78}Rb [13]) or triaxial (^{82}Y [4]) over a wide range of spins.

The $B(M1)$ strengths measured for the $\Delta I=1$ transitions in band 3 show the typical behavior observed in other odd-odd nuclei in this mass region. Relatively large (small) $M1$ strength resides in transitions where the favored (unfavored) signature states decay to the unfavored (favored) signature states, leading to an alternating pattern in the $B(M1)$ values, as shown in the bottom panel of Fig. 7. These alternating $B(M1)$ values are related to signature splitting [47–49] and can be explained in both the interacting boson-fermion approximation [50] and the particle-rotor coupling model [4]. A $\Delta I=1$ decay from a favored signature state involves only a realignment of the single-particle spin without altering the core spin and hence generates strong $M1$ radiation. The corresponding decay originating from an unfavored signature state requires a change in the core rotation (or boson number) which leads to reduced $B(M1)$ strength.

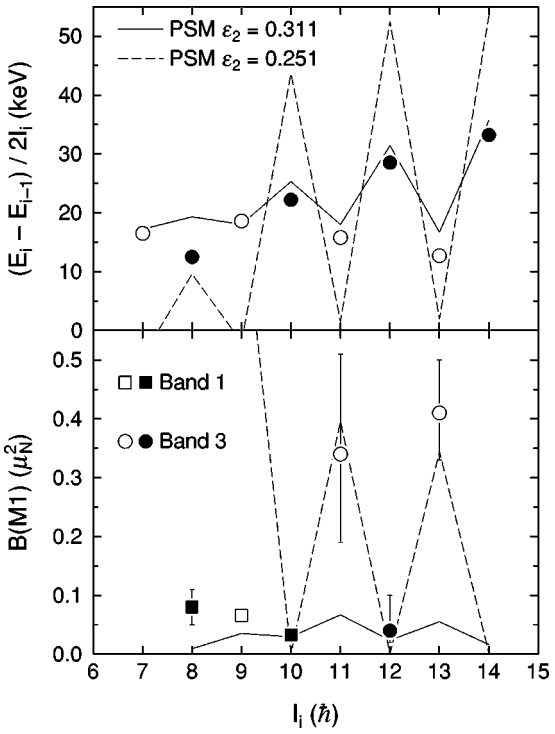

FIG. 7. Normalized energy differences between adjacent states in band 3 (top) and $B(M1)$ strengths in bands 1 and 3 (bottom) as a function of the initial-state spin I_i in ^{80}Y. Filled (open) symbols represent values with even (odd) I_i. The solid (dashed) curves represent the theoretical predictions from projected shell-model (PSM) calculations using quadrupole deformation $\epsilon_2=0.311$ ($\epsilon_2=0.251$). Not all available points at high spin are shown in the top portion of the figure.

Figure 7 also shows a comparison between the measured $B(M1)$ values in ^{80}Y with those predicted by the PSM calculations (see Sec. V A). Again, two sets of calculations with different deformations are presented. When the larger deformation ($\epsilon_2=0.311$) is used, the staggering in the signature splitting pattern is well reproduced for most of the measured states (top panel of Fig. 7). However, the overall magnitudes of $B(M1)$ are much smaller than the measured ones for transitions originating from odd-spin states, although the calculations reproduce the phase of the observed transitions. It is true, however, that the individual $B(M1)$ values measured for ^{80}Y are systematically smaller than those measured in the same spin range for both ^{78}Rb [13] and ^{82}Y [4]. This feature is predicted by the PSM [8], and may reflect the consistently larger collectivity displayed by ^{80}Y compared to either ^{78}Rb or ^{82}Y (see Fig. 6).

Nevertheless, we need to understand the reason why the PSM calculations with the model space constructed at deformation $\epsilon_2=0.311$ can provide fair agreement with the experimental energy spacings and Q_t values for this band, but cannot equally well describe the $B(M1)$ values. For this reason, we have performed another set of calculations in which a

smaller deformation $\epsilon_2=0.251$ is used. At this deformation, $g_{9/2}$ orbitals with smaller K components are close to the Fermi levels, making considerable contributions to an increase of the staggering amplitude in the $B(M1)$ pattern, in much better agreement with the experimental data. Thus, the calculations with a smaller deformation can reproduce nicely the observed $B(M1)$ data, while the agreement in the signature splitting pattern (top panel of Fig. 7) and the Q_t values (bottom panel of Fig. 6) becomes poor. On the other hand, calculations with deformations larger than $\epsilon_2=0.311$ provide increased Q_t values at the cost of worse agreement with the experimental energy spacings and $B(M1)$ values. At any rate, since $B(M1)$ strengths are sensitive to the single-particle attributes of the nuclear wave function, comparisons between the PSM predictions and the current experimental results can be used to reexamine the Nilsson model parameters appropriate for nucleon numbers in this mass region [51], as was done recently for proton-rich nuclei in the upper *fp* shell [52].

The collectivity of positive-parity band 5 was only determined roughly by two measured Q_t values and lower limits placed on three others in the band (based on effective lifetime measurements). Even so, it is clear that this structure, suggested to be based on the $\pi[422]5/2^+ \otimes \nu[431]1/2^+$ intrinsic configuration [23], is strongly deformed with β_2 values approaching 0.30 (assuming axial symmetry) near the middle of the band. However, this is not as deformed as what might be anticipated by the occupation of a quasineutron in the deformation-driving $[431]1/2^+$ orbital, which has been suggested to produce a more strongly deformed band ($\beta_2 \approx 0.4$) in ^{81}Sr [53].

Alternations in the intraband $B(M1)$ values have been observed for this band as well, following the same phase as those measured for band 3. They occur at spins where the signature splitting pattern becomes large in this band (see Fig. 11 in Ref. [15]). The magnitudes of the $B(M1)$ strengths appear to be larger than those for the same spin range in band 3, but it is difficult to draw any firm conclusions since two of the values obtained for band 5 are only lower limits.

D. Negative-parity bands

The deduced Q_t values for the yrast negative-parity band (band 1 in Fig. 1) are shown graphically as a function of initial-state spin in the bottom panel of Fig. 8. Their behavior with spin is qualitatively similar to that observed for the yrast positive-parity band (band 3 in Fig. 1). Values indicative of highly collective behavior are observed below the 11^- state, but then rather suddenly diminish above this spin, where they remain roughly constant up to the highest transitions for which Q_t values could be determined. Quantitatively, the average Q_t value of band 1 for spins less than 11 is slightly larger than those of the states in the same spin range in band 3, but the average values beyond the observed drop in each band are nearly identical. In general, the Q_t values are in good agreement with those predicted by CWS calculations before the observed drop occurs, but the agreement becomes significantly worse with increasing spin, as shown in Fig. 8.

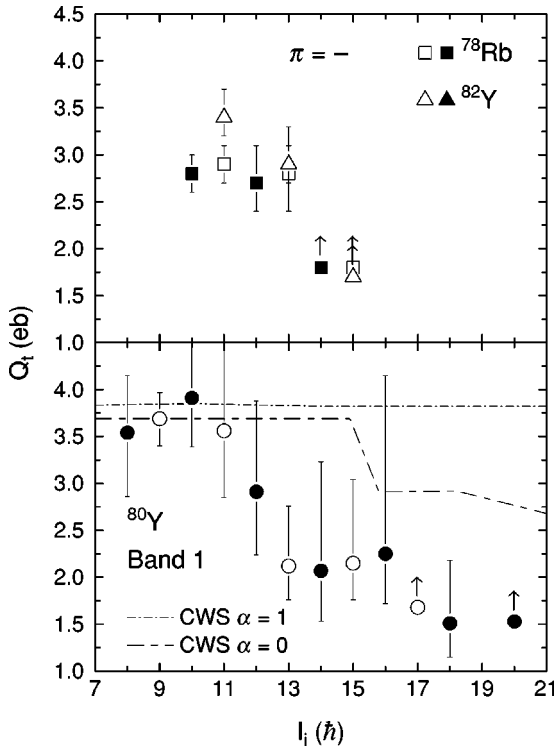

FIG. 8. Transition quadrupole moments Q_t as a function of initial-state spin I_i for the yrast negative-parity bands of ^{78}Rb [13] and ^{82}Y [4] (top), and yrast negative-parity band 1 in ^{80}Y (bottom). Filled (open) symbols represent values obtained from signature $\alpha=0$ ($\alpha=1$) transitions. Symbols with arrows indicate lower limits established from effective lifetimes. The broken curves represent the theoretical predictions for the $\alpha=0$ and $\alpha=1$ signatures inferred from cranked Woods-Saxon (CWS) calculations, as indicated in the figure.

The spin at which the drop in Q_t takes place corresponds roughly to the crossing frequency associated with a $g_{9/2}$ neutron alignment ($\hbar\omega \approx 0.64$ MeV) [15], as indicated by a sudden change in the $J^{(1)}$ moment of inertia at this point (see Fig. 10 of Ref. [15]). This is in good qualitative agreement with the predictions of the CWS calculations, which show evidence for a reduction in deformation following the initial development of a triaxial minimum near spin 16, a structure that continues clearly at higher spins (see Fig. 5). Evidently, qp alignment is responsible for the observed drop in Q_t, although it is a much sharper one than that of band 3 (see Sec. V C).

A similar drop in Q_t was also observed following a $g_{9/2}$ neutron alignment in the yrast negative-parity band in ^{81}Y [35]. On the other hand, falling Q_t values with increasing spin have not been observed in the lowest negative-parity bands of either ^{78}Rb [13] or ^{82}Y [4], as shown in the top panel of Fig. 8 (excluding the lower limits established from effective lifetimes). However, the measured Q_t values in these bands have not been measured to as high a spin as in ^{80}Y, and falling Q_t values have been predicted to occur at high rotational frequency in ^{78}Rb based on similar CWS calculations [13].

Associated with the first qp alignment in band 1 is a rather sudden increase in the amount of signature splitting observed

above the 16^- state, as indicated by larger alternations in a plot of the signature splitting pattern (see Fig. 11 in Ref. [15]). Such behavior is rather difficult to interpret theoretically because of mixing between different single-particle configurations, but it probably is a good indicator of structure changes. A similar (but perhaps more gradual) increase occurs in the signature splitting pattern of the yrast negative-parity band in ^{76}Rb near the point at which a proton band crossing was observed ($\hbar\omega = 0.69$ MeV) [54]. Increased alternations in the signature splitting pattern were accompanied by a phase reversal in the lowest negative-parity band of odd-odd ^{86}Nb [55]. Measurements of the Q_t moments in the spin region where this occurs (near spin 18) [34] show perhaps a slow corresponding fall in Q_t, but this decrease is certainly less sudden than that observed for ^{80}Y. However, comparisons between these two cases are difficult because it is likely that different intrinsic structures are involved, which may be reflected by the fact that a phase reversal does not occur in the ^{80}Y case.

The $B(M1)$ values measured for band 1 are shown in the bottom panel of Fig. 7. Unlike the yrast positive-parity band (band 3), there is a noticeable lack of an alternating pattern with spin, as is evident from the figure. In fact, there is an overall lack of consistency in the patterns of $B(M1)$ strengths with spin among the yrast negative-parity bands of ^{80}Y, ^{78}Rb [7,13], and ^{82}Y [4,11,12], demonstrating the difficulty in drawing any firm conclusions about the causes of their behavior. However, it is evident that the $B(M1)$ values measured for these three nuclei are weakest in the spin region where the signature splitting in the energy levels is also small. For the case of ^{78}Rb, the $B(M1)$ values do increase somewhat once a noticeable staggering forms in the signature splitting pattern above the 9^- state [7,13]. A similar comparison cannot be made for ^{80}Y since there have been no observed $M1$ transitions in the spin region ($I > 14$) where clear alternations develop in the signature splitting pattern [15].

The degree of collectivity of band 6 was determined roughly by a measurement of the Q_t values associated with two transitions, along with lower limits placed on the values associated with two other transitions (based on effective lifetime measurements). The two measured values are very similar (see Table II) and imply axial deformations of $\beta_2 \approx 0.26$. At this deformation, the most likely single-particle configuration for the unpaired proton and neutron yielding negative parity and band head spin-parity $I^\pi = 1^-$ is $\pi[422]5/2^+ \otimes \nu[301]3/2^-$, in agreement with a previous suggestion [23]. An alternative interpretation of the band-head configuration was suggested [15] as resulting from the coupling of the low-Ω $[431]1/2^+$ orbital with the $[301]3/2^-$ orbital. However, occupation of the $[431]1/2^+$ orbital by the unpaired proton (neutron) in ^{80}Y is unlikely unless the deformation exceeds $\beta_2 \approx 0.55(0.4)$ [41]. Either way, it is likely that the band-head configuration of this band actually consists of a complicated admixture of several Nilsson orbitals, as suggested previously [15]. It is difficult to use the results of CWS calculations to illuminate this issue any further, due to the complexity of the minima for non-yrast negative-parity states (see Sec. V B).

VI. SUMMARY

Lifetimes of 30 high-spin states in ^{80}Y were measured using the Doppler-shift attenuation method. The ^{54}Fe(^{28}Si, pn) reaction at 90 MeV, performed at the Florida State University (FSU) Tandem-Superconducting LINAC accelerator, was used to populate the excited states. The isotopically-enriched ^{54}Fe target was thick enough to stop completely all recoils and hence allowed for the analysis of line shape spectra. The FSU array consisting of ten Compton-suppressed Ge detectors (three of which were of the high-efficiency Clover design) was used to detect $\gamma-\gamma$ coincidences. Line shape spectra were obtained by gating from below the transition of interest. Lifetimes were measured by fitting theoretical line shapes to the experimental ones observed at both 35° and 145° whenever possible.

Transition quadrupole moments Q_t calculated from the lifetimes in the yrast positive-parity band change rather suddenly from an average value of 3.3 eb below spin 13 to 2.4 eb above this spin. These results are in fair qualitative agreement with the predictions of the projected shell model and cranked Woods-Saxon (CWS) calculations, which both indicate decreasing Q_t values with increasing spin. Total Routhian surfaces obtained from the CWS approach indicate the onset of a shape change from nearly prolate to triaxial at the point which the predicted decrease in Q_t occurs. A cranked shell-model analysis shows that this is likely caused by the gradual alignment of a $g_{9/2}$ proton pair. The measured magnetic dipole transition strengths $B(M1)$ show strong alternations between the two signatures, in qualitative agreement with the PSM calculations and neighboring odd-odd nuclei ^{78}Rb and ^{82}Y. The Q_t values for band 5 imply a structure having quadrupole deformation $\beta_2 \approx 0.30$ at low spin in an axial rotational model, in fair agreement with CWS calculations for non-yrast positive-parity states.

Decreasing Q_t values with increasing spin in the lowest yrast negative-parity band resemble closely those of band 3, except the magnitude of the average decrease is larger and occurs at perhaps a lower spin. CWS and cranked shell-model calculations together suggest this decrease is caused by the alignment of a $g_{9/2}$ neutron pair. Like band 3, this alignment is associated with a shape change from nearly prolate before the alignment to triaxial above the alignment, according to the CWS calculations. The intraband $B(M1)$ values are smaller than those of band 3 and show no alternating pattern with spin. The Q_t values for band 6 average 2.2 eb near the middle of the band, implying a modest axial deformation $\beta_2 \approx 0.26$ for this structure, which is smaller than that predicted by CWS calculations. This deformation favors a $\pi[422]5/2^+ \otimes \nu[301]3/2^-$ configuration for the band head, although highly mixed configurations are expected at high spin.

ACKNOWLEDGMENTS

This work was supported in part by the National Science Foundation (NSF) through Grant No. PHY-99-70991 (FSU) and an Indiana-Louis Stokes Alliance for Minority Participa-

tion Program (O.G.-U.). Y.S. acknowledges the support by the NSF under Contract No. PHY-0140324. We thank W. Nazarewicz for providing the results of his cranked Woods-Saxon calculations, and the staff of the FSU Tandem-Superconducting LINAC Facility for their support throughout the experiment. R.A.K. is grateful to S. Haring for providing support during the experiment and the writing of this manuscript.

[1] S. L. Tabor, Acta Phys. Hung. New Ser.: Heavy Ion Phys. **2**, 239 (1995).
[2] S. L. Tabor, Phys. Rev. C **45**, 242 (1992).
[3] A. J. Kreiner and M. A.J. Mariscotti, Phys. Rev. Lett. **43**, 1150 (1979).
[4] P. C. Womble, J. Döring, T. Glasmacher, J. W. Holcomb, G. D. Johns, T. D. Johnson, T. J. Petters, M. A. Riley, V. A. Wood, S. L. Tabor, and P. Semmes, Phys. Rev. C **47**, 2546 (1993).
[5] R. Zheng, S. Zhu, N. Cheng, and J. Wen, Phys. Rev. C **64**, 014313 (2001).
[6] I. Ragnarsson and P. B. Semmes, Hyperfine Interact. **43**, 425 (1988).
[7] R. A. Kaye, L. A. Riley, G. Z. Solomon, S. L. Tabor, and P. Semmes, Phys. Rev. C **58**, 3228 (1998).
[8] R. Palit, J. A. Sheikh, Y. Sun, and H. C. Jain, Phys. Rev. C **67**, 014321 (2003).
[9] K. Hara and Y. Sun, Int. J. Mod. Phys. E **4**, 637 (1995).
[10] J. W. Holcomb, T. D. Johnson, P. C. Womble, P. D. Cottle, S. L. Tabor, F. E. Durham, and S. G. Buccino, Phys. Rev. C **43**, 470 (1991).
[11] S. D. Paul, H. C. Jain, S. Chattopadhyay, M. L. Jhingan, and J. A. Sheikh, Phys. Rev. C **51**, 2959 (1995).
[12] G. D. Johns, K. A. Christian, R. A. Kaye, S. L. Tabor, G. García-Bermúdez, M. A. Cardona, A. Filevich, H. Somacal, and L. Szybisz, Phys. Rev. C **53**, 1541 (1996).
[13] R. A. Kaye, J. Döring, J. W. Holcomb, G. D. Johns, T. D. Johnson, M. A. Riley, G. N. Sylvan, P. C. Womble, V. A. Wood, S. L. Tabor, and J. X. Saladin, Phys. Rev. C **54**, 1038 (1996).
[14] G. García-Bermúdez, M. A. Cardona, A. Filevich, R. V. Ribas, H. Somacal, and L. Szybisz, Phys. Rev. C **59**, 1999 (1999).
[15] D. Bucurescu, C. A. Ur, M. Ionescu-Bujor, A. Iordăchescu, D. Bazzacco, F. Brandolini, G. de Angelis, M. De Poli, A. Gadea, S. Lunardi, N. Mărginean, N. H. Medina, D. R. Napoli, P. Pavan, C. Rossi Alvarez, and P. Spolaore, Nucl. Phys. **A705**, 3 (2002).
[16] C. Plettner, I. Ragnarsson, H. Schnare, R. Schwengner, L. Käubler, F. Dönau, A. Algora, G. de Angelis, D. R. Napoli, A. Gadea, J. Eberth, T. Steinhardt, O. Thelen, M. Hausmann, A. Müller, A. Jungclaus, K. P. Lieb, D. G. Jenkins, R. Wadsworth, and A. N. Wilson, Phys. Rev. Lett. **85**, 2454 (2000).
[17] C. J. Lister, P. E. Haustein, D. E. Alburger, and J. W. Olness, Phys. Rev. C **24**, 260 (1981).
[18] C. J. Lister, M. Campbell, A. A. Chishti, W. Gelletly, L. Goettig, R. Moscrop, B. J. Varley, A. N. James, T. Morrison, H. G. Price, J. Simpson, K. Connel, and O. Skeppstedt, Phys. Rev. Lett. **59**, 1270 (1987).
[19] J. H. McNeill, A. A. Chishti, W. Gelletly, B. J. Varley, H. G. Price, C. J. Lister, O. Skeppstedt, U. Lenz, C. J. Gross, J. Heese, and K. P. Lieb, Manchester University Progress Report 1987–1988, 1989 (unpublished), p. 20.
[20] D. Bucurescu, C. A. Ur, D. Bazzacco, C. Rossi-Alvarez, P. Spolaore, C. M. Petrache, M. Ionescu-Bujor, S. Lunardi, N. H. Medina, D. R. Napoli, M. De Poli, G. de Angelis, F. Brandolini, A. Gadea, P. Pavan, and G. F. Segato, Z. Phys. A **352**, 361 (1995).
[21] J. J. Ressler (private communication).
[22] P. H. Regan, C. Chandler, C. J. Pearson, B. Blank, R. Grzywacz, M. Lewitowicz, A. M. Bruce, W. N. Catford, N. Curtis, S. Czajkowski, P. Dessagne, A. Fleury, W. Gelletly, J. Giovinazzo, Z. Janas, C. Longour, C. Marchand, C. Miehe, N. A. Orr, R. D. Page, M. S. Pravikoff, A. T. Reed, M. G. Saint-Laurent, S. M. Vincent, R. Wadsworth, D. D. Warner, and J. S. Winfield, Acta Phys. Pol. B **28**, 431 (1997).
[23] J. Döring, H. Schatz, A. Aprahamian, R. C. de Haan, J. Görres, M. Wiescher, W. B. Walters, J. Rikovska, L. T. Brown, C. N. Davids, C. J. Lister, D. Seweryniak, and B. Foy, Phys. Rev. C **57**, 1159 (1998).
[24] C. Chandler, P. H. Regan, B. Blank, C. J. Pearson, A. M. Bruce, W. N. Catford, N. Curtis, S. Czajkowski, Ph. Dessagne, A. Fleury, W. Gelletly, J. Giovinazzo, R. Grzywacz, Z. Janas, M. Lewitowicz, C. Marchand, Ch. Miehé, N. A. Orr, R. D. Page, M. S. Pravikoff, A. T. Reed, M. G. Saint-Laurent, S. M. Vincent, R. Wadsworth, D. D. Warner, J. S. Winfield, and F. Xu, Phys. Rev. C **61**, 044309 (2000).
[25] A. Piechaczek, E. F. Zganjar, J. C. Batchelder, C. R. Bingham, T. N. Ginter, C. J. Gross, R. Grzywacz, B. D. Macdonald, S. D. Paul, K. Rykaczewski, and K. S. Toth, Phys. Rev. C **61**, 047306 (2000).
[26] J. J. Ressler, W. B. Walters, R. Grzywacz, J. C. Batchelder, C. R. Bingham, C. J. Gross, Z. Janas, M. Lipoglavsek, J. McConnell, S. D. Paul, A. Piechaczek, K. Rykaczewski, D. Radford, and J. Shergur, Phys. Rev. C **63**, 067303 (2001).
[27] A. Gavron, Phys. Rev. C **21**, 230 (1980).
[28] J. J. Ressler, A. Piechaczek, W. B. Walters, A. Aprahamian, M. Wiescher, J. C. Batchelder, C. R. Bingham, D. S. Brenner, T. N. Ginter, C. J. Gross, R. Grzywacz, D. Kulp, B. MacDonald, W. Reviol, J. Rikovska, K. Rykaczewski, J. A. Winger, and E. F. Zganjar, Phys. Rev. Lett. **84**, 2104 (2000).
[29] Yu. N. Novikov, H. Schatz, P. Dendooven, R. Beraud, Ch. Miehe, A. V. Popov, D. M. Seliverstov, G. K. Vorobjev, P. Baumann, M. J.G. Borge, G. Canchel, Ph. Desagne, A. Emsallem, W. Huang, J. Huikari, A. Jokinen, A. Knipper, V. Kolhinen, A. Nieminen, M. Oinonen, H. Pentillä, K. Peräjärvi, I. Piqueras, S. Rinta-Antila, J. Szerypo, Y. Wang, and J. Äystö, Eur. Phys. J. A **11**, 257 (2001).
[30] http://nucalf.physics.fsu.edu/~pavan/gnuscopehelp.html
[31] E. F. Moore, P. D. Cottle, C. J. Gross, D. M. Headly, U. J. Hüttmeier, S. L. Tabor, and W. Nazarewicz, Phys. Rev. C **38**, 696 (1988).
[32] J. F. Ziegler, J. P. Biersack, and U. Littmark, *The Stopping and Range of Ions in Matter* (Pergamon, New York, 1985).

[33] http://www.SRIM.org
[34] M. Wiedeking, R. A. Kaye, G. Z. Solomon, S. L. Tabor, J. Döring, G. D. Johns, F. Cristancho, M. Devlin, F. Lerma, D. G. Sarantites, I. Y. Lee, and A. O. Macchiavelli, Phys. Rev. C **62**, 024316 (2000).
[35] R. A. Kaye, C. T. Rastovski, S. L. Tabor, J. Döring, F. Cristancho, M. Devlin, G. D. Johns, I. Y. Lee, F. Lerma, A. O. Macchiavelli, D. G. Sarantites, and G. Z. Solomon, Phys. Rev. C **66**, 054305 (2002).
[36] M. Wiedeking, S. L. Tabor, F. Cristancho, M. Devlin, J. Döring, C. B. Jackson, G. D. Johns, R. A. Kaye, I. Y. Lee, F. Lerma, A. O. Macchiavelli, M. Naidu, I. Ragnarsson, D. G. Sarantites, and G. Z. Solomon, Phys. Rev. C **67**, 034320 (2003).
[37] Y. Sun and J. L. Egido, Nucl. Phys. **A580**, 1 (1994).
[38] A. A. Chishti, W. Gelletly, C. J. Lister, B. J. Varley, and Ö. Skeppstedt, J. Phys. G **16**, 481 (1990).
[39] T. D. Johnson, A. Raguse, C. J. Gross, M. K. Kabadiyski, K. P. Lieb, D. Rudolph, M. Weiszflog, T. Burkardt, J. Eberth, and S. Skoda, Z. Phys. A **350**, 189 (1994).
[40] H. Schnare, G. Winter, L. Käubler, J. Reif, R. Schwengner, J. Döring, G. D. Johns, S. L. Tabor, C. J. Gross, Y. A. Akovali, C. Baktash, D. W. Stracener, F. E. Durham, P. F. Hua, M. Korolija, D. R. LaFosse, D. G. Sarantites, I. Y. Lee, A. O. Macchiavelli, W. Rathbun, and A. Vander Molen, Phys. Rev. C **56**, 729 (1997).
[41] W. Nazarewicz, J. Dudek, R. Bengtsson, T. Bengtsson, and I. Ragnarsson, Nucl. Phys. **A435**, 397 (1985).
[42] R. Wyss, F. Lidén, J. Nyberg, A. Johnson, D. J.G. Love, A. H. Nelson, D. W. Banes, J. Simpson, A. Kirwan, and R. Bengtsson, Nucl. Phys. **A503**, 244 (1989).
[43] W. Nazarewicz, M. A. Riley, and J. D. Garrett, Nucl. Phys. **A512**, 61 (1990).
[44] J. Dudek, W. Nazarewicz, and P. Olanders, Nucl. Phys. **A420**, 285 (1984).
[45] I. Hamamoto and B. R. Mottelson, Phys. Lett. **132B**, 7 (1983).
[46] P. Ring, A. Hayashi, K. Hara, H. Emling, and E. Grosse, Phys. Lett. **110B**, 423 (1982).
[47] I. Hamamoto and H. Sagawa, Nucl. Phys. **A327**, 99 (1979).
[48] I. Hamamoto, Phys. Lett. **106B**, 281 (1981).
[49] F. Dönau, Nucl. Phys. **A471**, 469 (1987).
[50] P. Chowdhury, C. J. Lister, D. Vretenar, Ch. Winter, V. P. Janzen, H. R. Andrews, D. J. Blumenthal, B. Crowell, T. Drake, P. J. Ennis, A. Galindo-Uribarri, D. Horn, J. K. Johansson, A. Omar, S. Pilotte, D. Prévost, D. Radford, J. C. Waddington, and D. Ward, Phys. Rev. Lett. **67**, 2950 (1991).
[51] Y. Sun, R. Palit, J. A. Sheikh, R. A. Kaye, O. Grubor-Urosevic, S. L. Tabor, J. Döring, T. Baldwin, D. B. Campbell, C. Chandler, M. W. Cooper, S. M. Gerbick, C. R. Hoffman, J. Pavan, L. A. Riley, and M. Wiedeking (unpublished).
[52] Y. Sun, J. Zhang, M. Guidry, J. Meng, and S. Im, Phys. Rev. C **62**, 021601(R) (2000).
[53] E. F. Moore, P. D. Cottle, C. J. Gross, D. M. Headly, U. J. Hüttmeier, S. L. Tabor, and W. Nazarewicz, Phys. Lett. B **211**, 14 (1988).
[54] A. Harder, M. K. Kabadiyski, K. P. Lieb, D. Rudolph, C. J. Gross, R. A. Cunningham, F. Hannachi, J. Simpson, D. D. Warner, H. A. Roth, Ö. Skeppstedt, W. Gelletly, and B. J. Varley, Phys. Rev. C **51**, 2932 (1995).
[55] S. L. Tabor, J. Döring, G. D. Johns, R. A. Kaye, G. N. Sylvan, C. J. Gross, Y. A. Akovali, C. Baktash, D. W. Stracener, P. F. Hua, M. Korolija, D. R. LaFosse, D. G. Sarantites, F. E. Durham, I. Y. Lee, A. O. Macchiavelli, W. Rathbun, and A. Vander Molen, Phys. Rev. C **56**, 142 (1997).